Nanoscale

PAPER

CrossMark
← click for updates

Gallium plasmonic nanoparticles for label-free DNA and single nucleotide polymorphism sensing†

Antonio García Marín,‡[a] Tania García-Mendiola,‡[b,c] Cristina Navio Bernabeu,[c] María Jesús Hernández,[a] Juan Piqueras,[a] Jose Luis Pau,[a] Félix Pariente[b,c] and Encarnación Lorenzo*[b,c]

A label-free DNA and single nucleotide polymorphism (SNP) sensing method is described. It is based on the use of the pseudodielectric function of gallium plasmonic nanoparticles (GaNPs) deposited on Si (100) substrates under reversal of the polarization handedness condition. Under this condition, the pseudodielectric function is extremely sensitive to changes in the surrounding medium of the nanoparticle surface providing an excellent sensing platform competitive to conventional surface plasmon resonance. DNA sensing has been carried out by immobilizing a thiolated capture probe sequence from *Helicobacter pylori* onto GaNP/Si substrates; complementary target sequences of *Helicobacter pylori* can be quantified over the range of 10 pM to 3.0 nM with a detection limit of 6.0 pM and a linear correlation coefficient of R^2 = 0.990. The selectivity of the device allows the detection of a single nucleotide polymorphism (SNP) in a specific sequence of *Helicobacter pylori*, without the need for a hybridization suppressor in solution such as formamide. Furthermore, it also allows the detection of this sequence in the presence of other pathogens, such as *Escherichia coli* in the sample. The broad applicability of the system was demonstrated by the detection of a specific gene mutation directly associated with cystic fibrosis in large genomic DNA isolated from blood cells.

1. Introduction

The development of fast, sensitive and affordable methods for DNA sensing in clinical, food and environmental diagnostics has been the subject of intense research to date.[1,2] Of particular interest is the accurate detection of point mutations, so-called single nucleotide polymorphisms (SNPs), in the genetic material of different origins, since they are related to many important diseases and their identification is extremely important for making accurate clinical treatment decisions. Hence, different sensing-based strategies for SNP detection are reported aiming to develop reliable detection methods for application to routine analysis in biological samples. Among them, direct SNP detection, without the need for additional biomolecules or interacting agents, is ideal. However, most current assays in this sense still do not fulfill all requirements, although remarkable progress has been achieved in recent years. Thus, the development of simple and robust SNP sensing methods without the need for expensive equipment and reagents is in constant focus in research and industry.

Surface plasmon resonance (SPR) has shown very good results for label-free DNA and SNP detection. However, the excitation of plasmons has usually been done in thin films of noble metals[3–5] requiring complex optical coupling systems (prisms, gratings and optical waveguides) to excite plasmon waves. In addition, most of these systems reach detection limits in the micromolar range,[6,7] in particular concerning the detection of SNPs. Only a few studies reporting detection limits in the nanomolar range can be found in the literature.[8] In this sense, the use of localized surface plasmon resonance (LSPR) in plasmonic nanoparticles has the possibility of enhancing the sensitivity at the nanoscale, thus reducing the complexity of the optical set up in comparison to thin film technology, since the confinement of the electric field vibrations in a small volume can be achieved without coupling systems.[9] Coupling SPR with ellipsometry provides a sensitive and accurate technology for detection of biomolecules.[10,11] The ellipsometric functions (Ψ and Δ) present strong evidence of SPR excitation, particularly relevant for the Δ case, whose changes provide 10 times larger sensitivity than regular SPR in response to refractive index changes in the vicinity of the metal surface.[12–14]

[a]Grupo de Electrónica y Semiconductores, Departamento de Física Aplicada, Universidad Autónoma de Madrid, Spain
[b]Departamento Química Analítica y Análisis Instrumental, Universidad Autónoma de Madrid, Spain. E-mail: encarnacion.lorenzo@uam.es
[c]Instituto Madrileño de Estudios Avanzados (IMDEA) Nanociencia, Spain
†Electronic supplementary information (ESI) available. See DOI: 10.1039/c6nr00926c
‡These authors contributed equally to this work.

During the past few years, gallium nanoparticles (GaNPs) have arisen as potential competitors to expensive noble metals, such as gold and silver, whose resonance energies are found in the IR-visible wavelength range.[15–19] Several advantages have been found for nanostructures based on Ga, such as wide tunability of the resonance energy from the ultraviolet (UV) to infrared (IR) spectral region by varying their shape and size, simplicity of the preparation methods, and high sensitivity to the polarization of incident light.[20,21] Based on these properties, the effective use of GaNPs have been demonstrated in different applications, such as surface-enhanced Raman spectroscopy (SERS), fluorescence spectroscopy, and photo-induced degradation of biomolecules, showing ultraviolet (UV) local enhancement compared to Au or Ag nanoparticles.[22] GaNPs can be obtained by molecular beam epitaxy (MBE) and thermal evaporation on different substrates. A very thin layer of gallium oxide is formed from the oxidation of the NP surface after its exposure to the atmosphere, which helps to preserve a hemispherical shape.[23,24] The thickness of this shell has been estimated to be lower than 3.0 nm. These structures present significant bands in the pseudodielectric function obtained by external reflection ellipsometry at incidence angles of around 70°. Moreover, a characteristic behaviour in the pseudodielectric function is observed due to the increasing retardation of the p-component of the reflected beam with respect to the s-component as the incidence angle reduces. This effect leads to a reversal of polarization handedness (RPH), when the phase shift difference between both components of the light reaches 180° and occurs in a spectral range located between the resonance energies of in-plane and out-plane oscillatory modes. Ellipsometric studies in the arrays of small AgNPs have also shown RPH, but with weaker intensity than that observed on GaNPs.[25] Under the RPH condition, the pseudodielectric function is very sensitive to changes occurring in the medium surrounding GaNPs enabling its use in sensing platforms. Hence in a previous study,[26] GaNPs have been successfully employed by us for the development of an immunosensor. In the present work, we want to go a step forward applying this system to the development of a disposable and sensitive platform for DNA, SNP and gene mutation sensing. The analytical method relies on the fabrication of the sensing platform by GaNP deposition on silicon (Si) substrates followed by functionalization of the GaNP surface with a 5′-end hexamethylthiol-modified DNA capture probe and subsequent hybridization with the target DNA sequence. The hybridization event was detected by changes in the GaNP surrounding medium that gives rise to an energy shift in the pseudodielectric function under the RPH condition. The selectivity of the platform allows the detection of a single nucleotide polymorphism without the need for a hybridization suppressor in solution. A 12-mer specific DNA synthetic sequence of Helicobacter pylori (H. pylori), a bacterium that can cause digestive illness and even stomach cancer, has been chosen as a case study within the framework of developing approaches of broad applicability. In this sense, the developed biosensor can be an alternative to the classical gene assay, as the hybridization step is often required in the molecular diagnosis of human pathologies to detect mutations present within PCR products.

Cystic fibrosis is a genetic disease with autosomal recessive inheritance and a high global prevalence, which causes obstruction and recurrent infections of the respiratory tract associated with pancreatic insufficiency, often leading to a fatal outcome. It is caused by mutations in the cystic fibrosis transmembrane conductance regulator (CFTR) gene. Of over 1900 mutations described in this gene, the most common is the F508del,[27] which is a three-nucleotide deletion causing the loss of a phenylalanine residue of the CFTR protein. We have chosen the detection of this specific mutation in genomic DNA isolated from peripheral blood leukocytes from cystic fibrosis patients, as a case study to demonstrate the applicability of the developed biosensor to real sample sensing.

2. Results and discussion

2.1. Fabrication of the GaNP/Si platforms

GaNPs were deposited on Si (100) wafers as described in the Experimental section. A scan performed by SEM reveals (Fig. 1A) a fully-covered surface with hemispherical NPs. As shown in the cross-sectional image (Fig. 1B), the NPs were in direct contact with the substrate plane (with a contact angle close to 90°). The resulting histogram (Fig. 1C) shows a distribution with large NPs surrounded by smaller ones. Most of the NPs exhibited an average diameter below 50 nm. Beyond that, two groups of NPs are found, one between 50 and 175 nm, and the other between 225 and 275 nm. From the analysis of the SEM images, the interparticle distance between the largest NPs (larger than 200 nm) was estimated to be around 80 ± 20 nm.

X-ray diffraction analysis of the deposited GaNPs was performed in grazing incidence diffraction geometry. In that geometry, the diffraction allows us to study the crystal structure of a thin film on a substrate minimizing the substrate contribution due to the low penetration depth. The data was acquired under an incidence angle of 0.5° (see Fig. S1†). The spectra showed a broad band between 30 and 50 degrees when GaNPs were present (grey curve). The band did not show up in measurements taken on plain Si (black curve). The large band width is typical of low-crystallinity materials.[28] The band overlapped with the strongest diffraction lines in orthorhombic α-Ga (dashed vertical lines) and monoclinic β-Ga$_2$O$_3$ (dotted vertical lines), which are the most common phases under ambient conditions for Ga and Ga$_2$O$_3$. The diffraction angles were identified from the diffraction files (#00-005-0601 and #01-087-1901) of the International Centre for Diffraction Data (ICDD). Similar bands are obtained in the energy-dispersive X-ray diffraction of Ga droplets at temperatures above the freezing point (~150 K).[28] Thus, the results suggest that the inner volume of the GaNPs can remain in the liquid state for a long time without forming a uniform solid crystal phase.
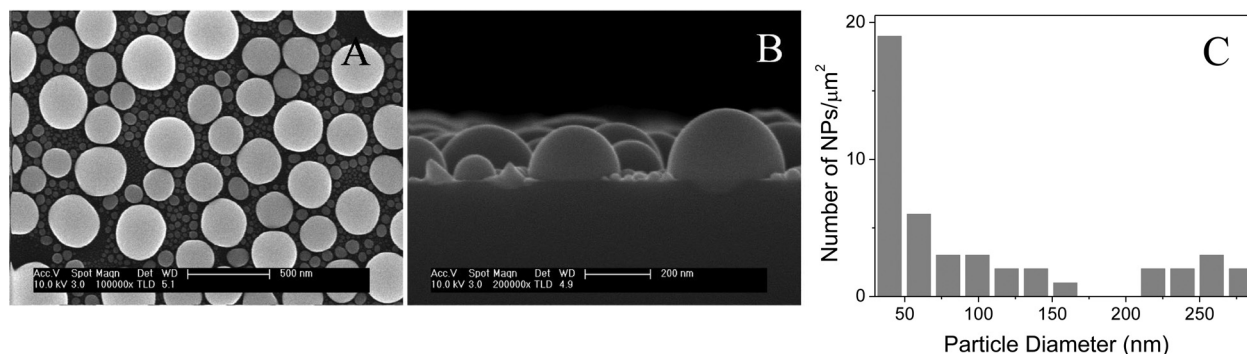
Fig. 1 (A) Top-view and (B) cross-sectional SEM images of the as-deposited GaNPs on Si substrates and (C) the corresponding histogram.

2.2. Ellipsometric characterization of GaNP/Si platforms

The experimental setup employed is represented in Scheme 1a. Ellipsometric functions psi (Ψ) and delta (Δ), defined as[29]

$$\rho = R_{P}/R_{S} = \tan \Psi \exp(i \cdot \Delta) \quad (1)$$

were obtained from the GaNP/Si platforms in the 1.5–4.5 eV range. Thus, ρ represents the ratio of the reflection coefficients R_{P} and R_{S} for light polarized in directions parallel (p) and perpendicular (s) to the plane of incidence, respectively. The tangent of Ψ is defined as the amplitude ratio between p- and s-components of the reflected beam, whereas Δ is the difference between the phase shifts for both polarization components. Besides these two, the ellipsometric analysis provides other parameters that are also relevant to analyze the plasmonic effects of GaNPs. To find the RPH condition, it is particularly useful to monitor the imaginary part of the

pseudodielectric function ($\langle \varepsilon_i \rangle$) which is defined under ambient conditions ($n = 1$) through:

$$\langle \varepsilon_i \rangle = \frac{\sin^2(\phi) \cdot \tan^2(\phi) \cdot \sin(4\Psi) \cdot \sin(\Delta)}{(1 + \sin(2\Psi) \cdot \cos(\Delta))^2} \quad (2)$$

where ϕ is the incidence angle.[29] In complex systems, such as multilayers, plasmonic structures on a substrate, *etc.*, each of the different parts of the system contributes to the dielectric response. In GaNP systems, $\langle \varepsilon_i \rangle$ gives information on the optical properties of the whole NP–substrate system and has been used to monitor the plasmonic resonance of these particles.[30,31]

Ellipsometric analysis of GaNPs supported on different substrates has been typically carried out at the Brewster's angle for Si surfaces (70°).[20,32,33] Those measurements have revealed the presence of two resonant modes, separated by several electron volts in GaNP systems, as a result of its hemispherical geometry. However, lower angles have been hardly studied in these systems. Fig. 2A shows $\langle \varepsilon_i \rangle$ spectra measured in the 70–50°
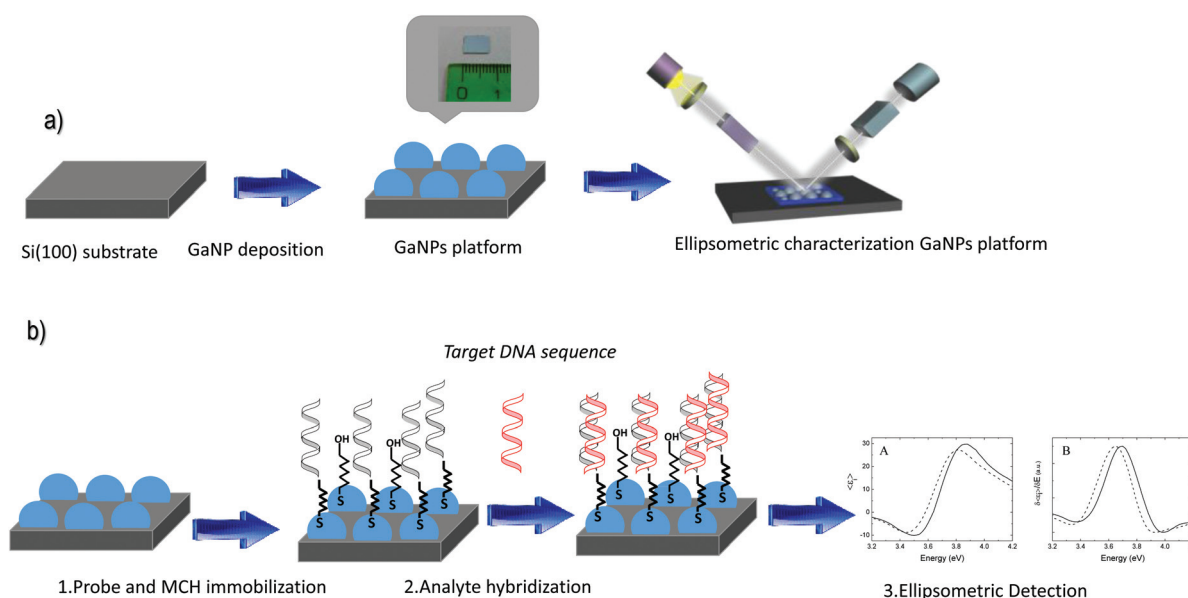
Scheme 1 Schematic representation of the: (a) fabrication of the GaNP/Si platform and (b) DNA biosensor development.
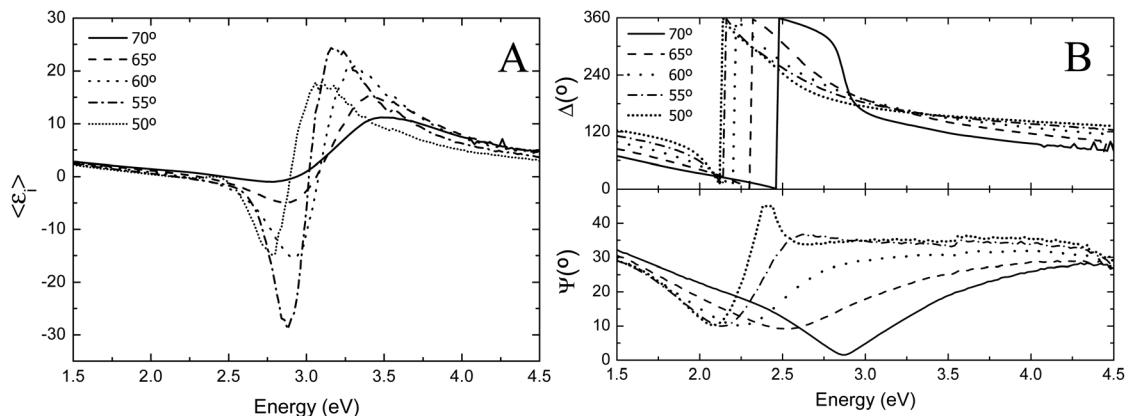
Fig. 2 (A) $\langle \varepsilon_i \rangle$ and (B) Ψ and Δ functions at incidence angles between 70° and 50° for a GaNP/Si platform with an estimated average diameter of 250 nm for the largest NPs.

range. As can be observed, there is an abrupt sign change at around 3.0 eV, which becomes very steep at 55°. According to eqn (2), the numerator is nullified at energies close to 3.0 eV in these samples, when Δ is 180°, as can also be observed in Fig. 2B. The physical meaning is that, in the case of an elliptically polarized beam impinging on the sample surface at this energy and incidence angle, the reflected beam has a polarization vector that rotates in the opposite direction to the polarization vector of the incident beam. This condition is called RPH and it has been demonstrated to be very sensitive to the adsorption of biomolecules.[26] Eqn (2) takes negative values when Δ is higher than 180°, that is, sin(Δ) ranges between 0 and −1. Around the RPH condition, a characteristic line-shape arose in the $\langle \varepsilon_i \rangle$ spectra whose energy and maximum amplitude depend on the NP size and the substrate used as the incidence angle decreased from 70° to 50°. To optimize the amplitude when Δ is 180°, it is required to change the incidence angle until Ψ approaches 45° in order to minimize the value of the denominator 1 + sin(2Ψ)·cos(Δ) in eqn (2). Under these conditions, the ellipticity of the polarization is preserved upon reflection on the nanostructured surface.

In order to obtain better sensitivities, it is recommended to have a steeper increase around the RPH condition. The large separation between in-plane and out-of-plane resonant modes in GaNPs contributes to enhance the phase difference between the p- and s-polarization components in the reflected beam, yielding a large peak-to-peak amplitude around the RPH condition in comparison to other nanostructures. For studying surface interactions in our ellipsometric setup, an incidence angle of 55° was chosen to maximize the peak-to-peak amplitude. The DNA biosensor developed is based on the quantification of spectral changes observed in the pseudodielectric function around the RPH condition, in particular, the energy shift of the inflection point (δE).

2.3.   DNA biosensor development

The biosensor construction is depicted in Scheme 1b. The first step was the immobilization of the 5′-end hexamethylthiol DNA capture probe on the GaNP/Si platform. In a first approach, a single 12-mer sequence from the *H. pylori* (HP1-SH) was immobilized on the platform through the thiol group following the procedure described in the Experimental section. After this step, the subsequent immobilization of 6-mercapto-1-hexanol (MCH) was carried out. This short thiol chain acts as a lateral spacer in order to avoid unspecific interactions between the probe and the platform surface and keep the probe standing up, with the bases available for the hybridization event with the corresponding target DNA chain. The whole process was monitored using ellipsometry. Fig. 3A shows the $\langle \varepsilon_i \rangle$ spectra of a GaNP/Si platform before and after modification with the HP1-SH probe and the probe/MCH as described in the Experimental section. As can be seen there is an energy shift of the inflection point (δE) around the RPH condition before and after successive modifications. In order to definitively find the inflection point, the derivative of the spectra in Fig. 3A was taken with respect to energy ($\partial \langle \varepsilon_i \rangle / \partial E$) (see Fig. 3B). For the sake of clarity the maximum of these spectra was normalized to 1. As can be seen in Fig. 3B, the values obtained for the energy shift were 30 ± 5 and 50 ± 10 meV after the modification with the HP1-SH probe and further modification with the MCH, respectively.

In order to assess that the δE changes observed were only due to the immobilization of the probe onto GaNPs, and not due to changes in environmental conditions, the effect of temperature on the RPH condition was evaluated. To this end, the $\langle \varepsilon_i \rangle$ spectra of an unmodified GaNP/Si platform was measured before and after keeping it at different temperatures, ranging from 4 °C to 40 °C, for 1 hour. No significant changes were observed. Since NP functionalization and the following hybridization were performed at these temperatures (4 °C and 40 °C, respectively), one can affirm that δE is strictly caused by the chemical modification of the NPs.

The effect of the HP1-SH concentration (from 0.010 to 20 μM) in the $\langle \varepsilon_i \rangle$ spectra was also evaluated. Fig. 4 shows the δE values *versus* probe concentration. It is evident that δE increases on increasing HP1-SH until 2.0 μM and then levels
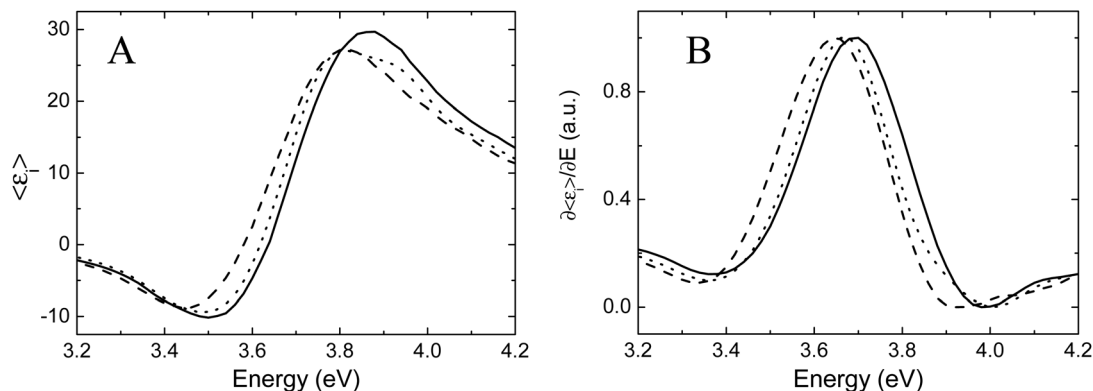
Fig. 3 (A) $\langle \varepsilon_i \rangle$ spectra of a GaNP/Si platform before (black line) and after modification with: the HP1-SH probe (dotted line) and the probe/MCH (dashed line). (B) $\partial \langle \varepsilon_i \rangle / \partial E$ of a GaNP/Si platform before (black line) and after modification with the HP1-SH probe (dotted line) and the probe/MCH (dashed line).
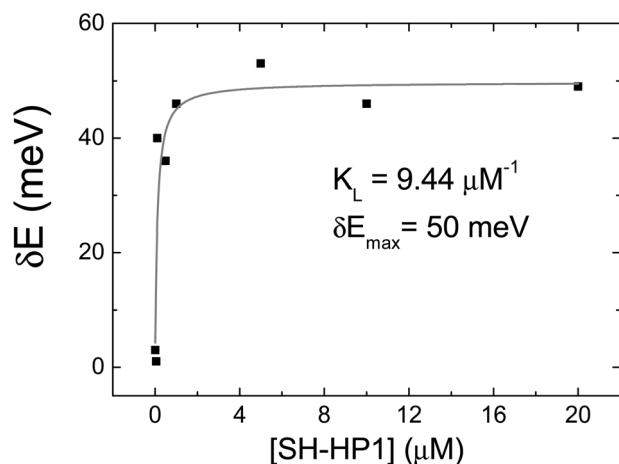

Fig. 4 Representation of δE versus the DNA capture probe concentration. Fitting results obtained from the fitted Langmuir isotherm (grey line) are also included.

off. The data were optimally fitted to a Langmuir isotherm equation:

$$\delta E = \frac{\delta E_{\max} \cdot K_L \cdot c}{1 + K_L \cdot c} \qquad (3)$$

where $\delta E_{\max}$ is the largest δE value measured in energy units, K_L is the Langmuir constant and c is the probe concentration. The fitting curve gave rise to a K_L and a $\delta E_{\max}$ of 9.44 μM^{-1} and 50 meV, respectively.

From the above results, it can be concluded that a HP1-SH concentration of 2.0 μM was chosen for the biosensor preparation, since this value was in the plateau where higher concentrations would hardly improve the response, whereas lower concentrations could reduce DNA hybridization sites and, thus, sensor sensitivity. Moreover, the isotherm seems to indicate that immobilization of HP1-SH onto the GaNP/Si platform takes place forming a monolayer, like on gold surfaces.[34] In order to support the evidence of a thiolated species on the

GaNP/Si platform, XPS analysis was performed before (reference substrate) and after modification of the platform with the probe and MCH. XPS overview spectra (Fig. S2†) of the modified platform show a S 2s core level at 227 eV, whereas no evidence of the S 2s core level is observed in the reference substrate. Only one chemical state is observed, which indicates one type of bond between the S (from the thiol group) and the GaNPs. The S 2p does not appear because it was overlapped with the Ga 3s high binding energy tail side.

The potential use of the probe functionalized GaNP/Si platforms (MCH/HP1-SH–GaNPs) as a nucleic acid biosensing system was evaluated through hybridization assays, according to the procedure described in the Experimental section. In the first hybridization test, 0.50 nM of a complementary (HP2$_C$) and a non-complementary (HP2$_{NC}$) sequence of *H. pylori* were used as the DNA target. The corresponding signals before and after hybridization are shown in Fig. 5A. As can be seen, hybridization of the probe with the HP2$_C$ in the biosensor recognition layer resulted in a considerable shift in δE (72 ± 7 meV), whereas virtually no changes ($\leq$10 meV) were observed for the HP2$_{NC}$. The magnitude in the δE shift is around 7 times higher when the HP2$_{NC}$ sequence is used compared to that obtained with HP2$_{NC}$, indicating that a target sequence of the *H. pylori* DNA fragment can be specifically detected using the developed biosensing platforms. Different platforms modified with the probe, prepared by the same manner, were incubated with increasing concentrations of HP2$_C$ from 10 pM to 3.0 nM. The changes in δE increased on increasing the amount of the target sequence. As can be seen in Fig. 5B, there is a fairly linear correlation between the signal and the increasing amount of HP2$_C$ over all ranges studied, with a linear correlation coefficient of R^2 = 0.990. The detection limit, calculated as the ratio between three times the standard deviation of the background signal and the sensitivity, was determined to be 6.0 pM. The reproducibility of the biosensor was determined by measuring the response of five different devices prepared using the same protocol (MCH/HP1-SH–GaNPs) and exposed to 0.5 nM HP2$_C$. The relative standard deviation (RSD) of the δE was found to be 3.4%.
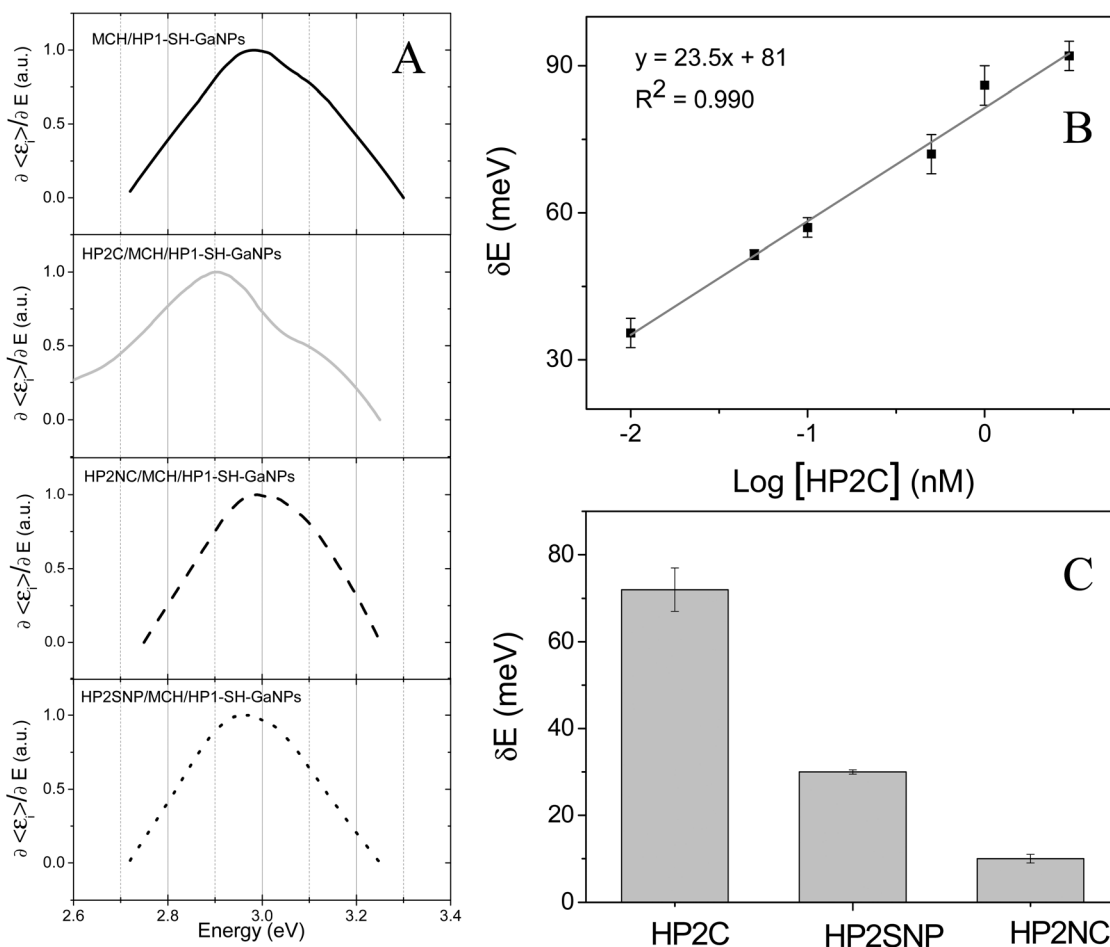
Fig. 5 (A) $\partial\langle\varepsilon_i\rangle/\partial E$ of a GaNP/Si platform modified with the HP1-SH capture probe and MCH, before (black line) and after the hybridization event in the presence of a complementary, HP2$_C$ (grey line), non-complementary, HP2$_{NC}$ (dashed line) and single nucleotide polymorphism sequence, HP2$_{SNP}$ (dotted line). (B) Representation of δE *versus* the complementary sequence concentration. The fitting curve and equation are also included. (C) Bar diagram of the energy shift (δE) after hybridization with the HP2$_C$, HP2$_{SNP}$, HP2$_{NC}$ sequence. The data are the average of five determinations and the error bars represent the standard deviation.

2.3.1. SNP and selective DNA sequence detection. The selectivity of the biosensor was evaluated by using as target a sequence containing a single nucleotide polymorphism (HP2$_{SNP}$) under the same hybridization conditions employed for the perfectly matched sequence. The hybridization with the single mismatched sequence would give a distorted double-helix, which can be detected by the changes in the optical properties of the sensing layer. Based on this, one would anticipate a different biosensor response when compared to hybridization with HP2$_C$. Fig. 5A shows the $\langle\varepsilon_i\rangle$ spectrum of a platform modified with the probe before and after hybridization with 0.50 nM HP2$_{SNP}$. As can be seen, the presence of the mutation causes a decrease in the energy shift. From the responses of five biosensors an average value of the energy shift of 30 ± 5 meV was observed, which is less than half of the energy shift of 72 ± 7 meV observed when the biosensors respond to 0.50 nM of a perfectly matched sequence HP2$_C$ (see Fig. 5C). Since the error associated with each measurement is less than 5%, it can be concluded that the developed sensing
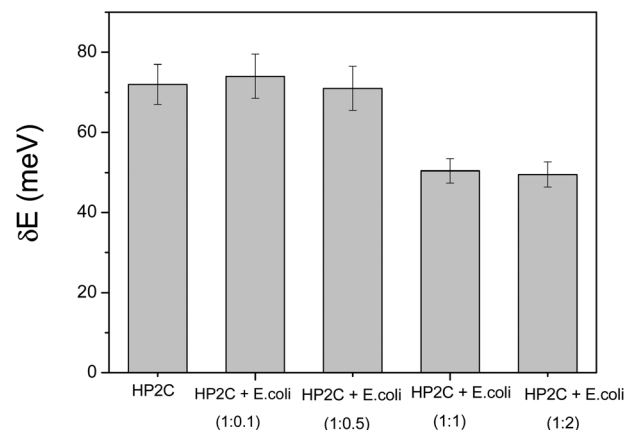

Fig. 6 Bar diagram of the δE after hybridization with 0.5 nM of *H. pylori* and with 0.5 nM of *H. pylori* + increasing concentrations of an *E. coli* sequence (HP2$_C$ + *E. coli*): 0.05 nM, 0.25 nM, 0.5 nM and 1.0 nM. The data are the average of five determinations and the error bars represent the standard deviation.

system is able to unambiguously detect the presence of a SNP in a given sequence at a nanomolar (nM) concentration, without the need for stringent conditions (*i.e.* formamide) usually employed for such purposes.

Concerning selectivity, another important aspect to take into account for analytical application of DNA sensing devices is the effect on the response of other sequences present in the sample that can act as potential interferents. In order to assess if the developed biosensing device can detect a specific DNA

sequence in a sample containing other sequences besides the target, the biosensor response to samples containing both *H. pylori* and *Escherichia coli* (*E. coli*) sequences, at different concentrations, was also evaluated. Fig. 6 shows the bar diagram of the results. As can be seen, the presence of *E. coli* at lower concentrations (from 0.05 nM to 0.25 nM) than the target does not affect the biosensor response. When the *E. coli* sequence is present at high concentrations (0.5 nM and 1.0 nM), the biosensor response decreases about 30%. From these

Table 1 Sequences amplified by PCR of the genomic DNA samples used in this work

| PCR samples		
Wild type sequence	5′-AACCGATTGAATATGGAGCCAAATATATAATTTGGGTAGTGTGAAG GGTTCATATGCATAATCAAAAAGTTTTCACATAGTTTCTTACCTCTTCT AGTTGGCATGCTTTGATGACGCTTCTGTATCTATATTCATCATAGGAA ACACCAAAGATGATATTTTCTTTAATGGTGCCAGGCATAATCCAGGAA AACTGAGAACAGAATGAAATTCTTCCACTGTGCTTAATTTTACCCTCT GAAGGCTCCAGTTCTCCCATAATCACCATTAGAAGTGAAGTCTGGAAA TAAAACCCATCATTATTAGGTCATTATCAAATCACGCTCAGGATTCAC TTGCCTCCAATTATCATCCTAAGCAGAAGTGTATATTC	WT
Mutated sequence	5′-AACCGATTGAATATGGAGCCAAATATATAATTTGGGTAGTGTGAAG GGTTCATATGCATAATCAAAAAGTTTTCACATAGTTTCTTACCTCTTCT AGTTGGCATGCTTTGATGACGCTTCTGTATCTATATTCATCATAGGAA ACACCA__ATGATATTTTCTTTAATGGTGCCAGGCATAATCCAGGAAA ACTGAGAACAGAATGAAATTCTTCCACTGTGCTTAATTTTACCCTCTG AAGGCTCCAGTTCTCCCATAATCACCATTAGAAGTGAAGTCTGGAAAT AAAACCCATCATTATTAGGTCATTATCAAATCACGCTCAGGATTCACT TGCCTCCAATTATCATCCTAAGCAGAAGTGTATATTC	MUT
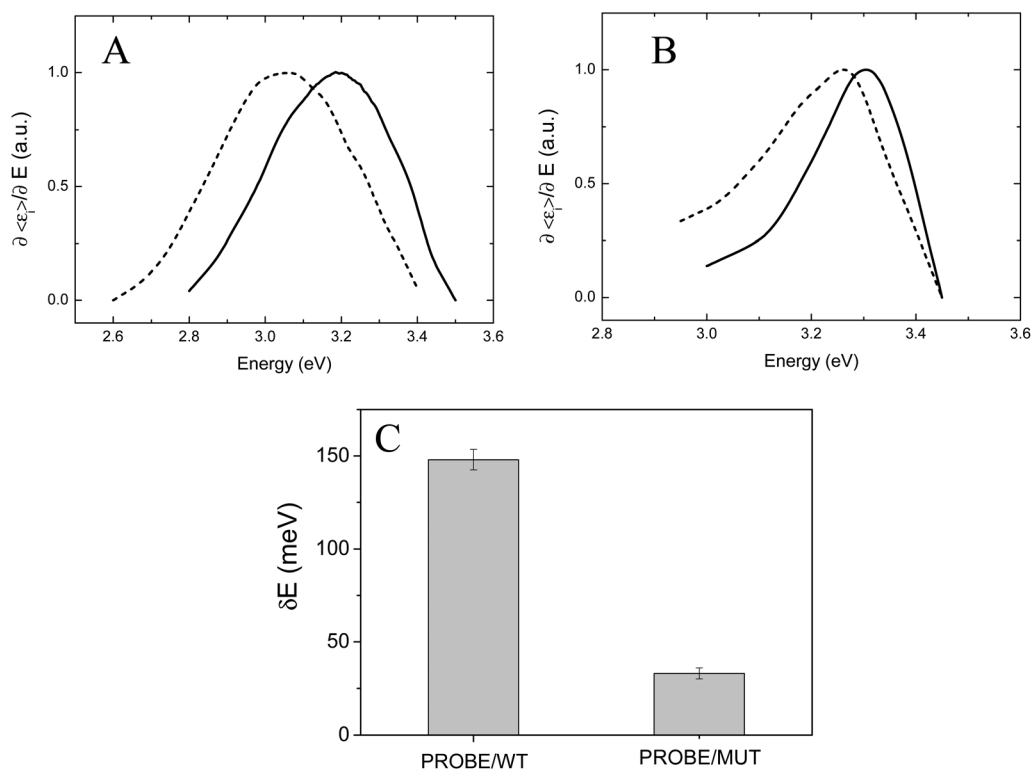
Fig. 7 $\partial\langle\varepsilon_i\rangle/\partial E$ of a GaNP/Si platform modified with the HP1-SH capture probe and MCH, before (black line) and after (dotted line) the hybridization with the wild (A) and mutated (B) type sequence. Bar diagram (C) of the δE before and after hybridization with the WT and the MUT sequences. The data are the average of five determinations and the error bars represent the standard deviation.

results, it can be concluded that it is possible to detect the target sequence in the presence of other pathogens present in the sample.

2.4. Detection of gene mutation in real genomic DNA

In order to assess the broad applicability of the biosensor developed, in particular while working with real genomic DNA, we have gone a step forward and applied it to the detection of gene mutation in human genomic DNA extracted from blood cells. As a case study we have chosen one specific mutation associated with cystic fibrosis, the F508del. This mutation, which is one of the most common mutant alleles, consists in a deletion of three bases (CTT) at the 508 position of the CFTR mRNA.

The genomic DNA samples were isolated from peripheral blood leukocytes and amplified by PCR (see Table 1, Experimental section). Mutation detection is accomplished directly in a 373 bp sequence from exon 11 in the CFTR gene, following a similar procedure to that described above for the *H. pylori*. A thiolated wild type (WT-SH) synthetic probe (100 bp) was immobilized onto the GaNP/Si platform surface following the procedure described in the Experimental section.

The modification of the GaNP/Si platform with the WT-SH probe/MCH causes an energy shift of the inflection point (δE) of 105 ± 0.05 meV. This value is higher than that observed in the case of *H. pylori*, suggesting that the larger size of the immobilized capture probe involves a larger δE. Hybridization with the wild (WT) or mutated (MUT) type target causes an additional energy shift. Fig. 7 shows the spectra of the platform modified with the probe before (black line) and after (dotted line) hybridization with the wild type (A) and mutated type (B). The energy shift is around 5 times higher in the case of the fully matched wild type sequence (see the bar diagram of Fig. 7C), which allows perfect discrimination between the wild type and the mutated form of the gene in the study. The reproducibility of the developed methodology was evaluated by the response of five different biosensors (prepared in the same manner, immobilizing 5 μL of a 2.0 μM WT-SH) to 5 μL of 50.0 pg per μL of either WT or MUT target DNA. Reproducible signals with a RSD less than 5% for both targets were obtained.

The results were validated by DNA sequencing. The agreement between the data obtained by both methodologies demonstrates that the developed system can be applied to detect gene mutations directly in DNA real samples. The method developed can be competitive to conventional surface plasmon resonance concerning sensitivity and selectivity with the advantage that simpler and cheaper optical equipment is required.

3. Conclusions

The DNA biosensing platform developed, based on the spectral changes of the pseudodielectric function of GaNP/Si platforms, is a selective one that allows the detection of, not only a determined sequence, but also the presence of a SNP in that sequence. Moreover, the target DNA detection is possible in the presence of a potential interferent. Accurate detection of point mutations is of great interest, since it is well known that these mutations can play a significant role in the onset and development of many types of cancer and cystic fibrosis, among other diseases. The developed DNA biosensor platform has broad applicability. This has been demonstrated by the detection of a SNP in a synthetic sequence of *H. pylori*, and the detection of a specific gene mutation in the cystic fibrosis transmembrane conductance regulator (CFTR) gene directly in PCR amplicons extracted from blood cells. The results obtained demonstrate that the developed sensors are very useful for rapid and specific detection of mutations in PCR amplified products without complicated sample treatment procedures. The present work represents a powerful new and versatile analytical tool for detecting SNP and mutations in synthetic and PCR real DNA samples.

4. Experimental section

4.1. Materials

99.9999% pure gallium (Ga) was acquired from Goodfellow (England). 6-Mercapto-1-hexanol (MCH) and all other chemicals used in this work were of reagent grade quality, obtained from Sigma-Aldrich Co., and used as received without further purification. The custom-made sequences were supplied by Sigma-Aldrich Co.

Several synthetic oligonucleotides were used in this work. In a first approach the 5′-end hexamethylthiol 12-mer sequence, 5′-SH $(CH_2)_6$–CAAAGGGCAGGA (denoted as HP1-SH) from the *Helicobacter pylori* (*H. pylori*) bacterium was used as a capture probe to modify the GaNP/Si platforms. To carry out the analytical strategy the following synthetic sequences were used: the fully complementary sequence 5′-TCCTGCCCTTTG (denoted as $HP2_C$), the non-complementary sequence 5′-CAAG-TAAAGGGC (denoted as $HP2_{NC}$) and the single nucleotide polymorphism located at the middle of the sequence 5′--TCCTACCCTTTG (denoted as $HP2_{SNP}$). As an interfering agent, a sequence from the pathogen bacterium *Escherichia coli* 5′-TGCCGCTCATCC GCCACATATCCTG (denoted as *E. coli*) was used.

To carry out the determination of real genomic DNA samples a synthetic 5′-end hexamethylthiol modified 100-mer sequence from exon 11 of the cystic fibrosis transmembrane conductance regulator (CFTR) gene, was used as a capture probe to modify the GaNP/Si platforms. This sequence, denoted as WT-SH, is as follows: 5′-HS $(CH_2)_6$-TCTCAG-TTTTCCTGGATTATGCCTGGCACCATTAAAGAAAATATCATCTTT-GGTGTTTCCTATGATGAATATAGATACAGAAGCGTCATCAAAGCA-TGCC.

Genomic DNA employed as a target was isolated from peripheral blood leukocytes from cystic fibrosis patients by standardized procedures (commercial QAIquick extraction, Kit Purogene from Qiagen GmbH, Hilden, Germany) as we pre-

viously described.[35] For all patients, informed consent was obtained. Intronic primers were designed to amplify the exon 11 and flanking intronic sequences of the CFTR gene. The PCR product was electrophoresed in 1.5% agarose gel in Tris-borate-EDTA, and bands detected with ethidium bromide. Before using the samples, which consisted of 373 bp wild type or complementary (WT) and 370 bp mutated (MUT) sequences (see Table 1), they were purified with the QAIquick extraction kit according to the manufacturer's instructions to remove traces of buffer, primers and deoxy-NTP. Moreover, all amplicons were validated by sequentiation methods in the Medical and Molecular Genetics Institute (INGEMM) of Madrid (Spain), which supplied the samples.

Sequencing of DNA samples was carried out using a Sanger Sequencher 3730xL, arrays 36 cm, POP 7, Applied Biosystems. The final concentration was determined by UV-visible molecular absorption spectrometry using a Thermo Scientific Nano-Drop™ 1000 spectrophotometer (NanoDrop Technologies). PCR fragments were generated in a BIO-RAD thermal cycler (DNA Engine Tetrad2, Peltier Thermal Cycler, BIO-RAD Laboratories Inc.).

All solutions were prepared just prior to use. Water was purified with a Millipore Milli-Q-system (18.2 MΩ cm) and was sterilized with a Nüve OT 012 small steam autoclave.

4.2. GaNP deposition

GaNPs are obtained by directly depositing Ga on Si(100) wafers with a Joule-effect thermal evaporator under a constant electrical current for 2 minutes. Prior to Ga deposition, the substrates are cleaned with a HF/H_2O solution to etch the native oxide. The evaporator includes an ice-cooled heat sink placed in contact with the substrate in order to maintain a constant temperature near zero degrees Celsius and improve the reproducibility of size distributions for different evaporations deposited under the same conditions. The GaNP-covered wafer is cleaved into different pieces of about 0.4 cm^2 for use in the remaining experiments.

4.3. Scanning electron microscopy characterization

The morphology of the GaNP/Si platforms was studied using a field-effect scanning electron microscopy (SEM) at 10 kV with an Everhart–Thornley secondary-electron detector.

4.4. X-ray diffraction analysis

Measurements were performed in an X'Pert PRO diffractometer from Panalytical with a theta/theta configuration at an incidence angle of 0.5°. The as-evaporated GaNP/Si platform was measured immediately after the Ga deposition. For the plain Si wafer that serves as a reference, the native oxide was chemically etched before measurement with a water diluted hydrofluoric acid (HF/H_2O) solution.

4.5. X-ray photoelectron spectroscopy

Measurements were performed under Ultra High Vacuum conditions (UHV, with a base pressure of 5×10^{-10} mbar) using a monochromatic Al K-alpha line as the exciting photon source

(1486.7 eV), and a hemispherical energy analyzer (SPHERA-U7, the analyzer pass energy was set to 20 eV for the XPS measurements to have a resolution of 0.6 eV). In order to compensate for the built up charge on the sample surface during the measurements, it was necessary to use a Flood Gun (FG-500, Specs) with low energy electrons of 3 eV and 40 μA.

4.6. Ellipsometric measurements

Samples are measured at room temperature using a Jobin Yvon UVISEL spectroscopic phase-modulated ellipsometer in external reflection mode with modulator and analyzer angles set at 0 and 45°, respectively. The incidence angle was maintained at 55° and energies between 1.5 and 4.5 eV were used for the present work. The light spot on the sample surface has an elliptical shape with a 6.6 mm × 4.0 mm size at that incidence angle.

4.7. Immobilization of the thiolated DNA capture probe on GaNP/Si platforms

Prior to the probe immobilization, the as-deposited GaNP platforms were carefully selected in order to have a peak-to-peak amplitude of 40 ± 2 and an RPH energy in the range of 3.0–3.7 eV. Then, 20 μL of a 2.0 μM thiolated capture probe (HP1-SH or WT-SH) solution were transferred onto the clean GaNP/Si platform and it was kept standing for 1 h at 4 °C. Afterwards, the oligonucleotide functionalized GaNP platform (HP1-SH–GaNPs or WT-SH–GaNPs) was immersed in a 1.0 mM MCH solution for 1 h and the resulting MCH/HP1-SH–GaNP or MCH/WT-SH–GaNP platform was thoroughly washed with sterile water for 30 min to remove unspecific adsorbed DNA. Finally, the sensing platform was dried with N$_2$.

4.8. Denaturation of PCR DNA samples

Real PCR DNA amplicons were denatured before the hybridization step by immersing them in boiling water (100 °C) for 30 minutes followed by rapid cooling in an ice bath.[36]

4.9. Hybridization and SNP or mutation detection

MCH/HP1-SH–GaNP or MCH/WT-SH–GaNP sensing platforms were subsequently hybridized (1 h, 40 °C) with 20 μL of hybridization solution (0.4 M NaCl) containing: 0.50 nM of complementary, non-complementary or single base-pair mismatched sequences, in the case of *H. pylori*, or 50 pg per μL of wild type (WT) or mutated (MUT) in the case of denatured real PCR amplicons. The sensing platforms were then immersed in nuclease free sterile water for 30 min and dried with N$_2$ before taking the ellipsometric measurements.

Acknowledgements

thank Isidoro Poveda and Noemí González from the Inter-department Research Service (SIdI-UAM) facilities for the SEM and X-ray diffraction measurements.

References

1 M. J. Heller, *Annu. Rev. Biomed. Eng.*, 2002, **4**, 129–153.

2 B. L. Poe, D. M. Haverstick and J. P. Landers, *Clin. Chem.*, 2012, **58**, 725–731.

3 R. B. M. Schasfoort and A. J. Tudos, *Handbook of surface plasmon resonance*, RSC Publishing, Cambridge, 2008.

4 W. A. Murray and W. L. Barnes, *Adv. Mater.*, 2007, **19**, 3771–3782.

5 J. Homola, S. S. Yee and G. Gauglitz, *Sens. Actuators, B*, 1999, **54**, 3–15.

6 P. K. Wilson, T. Jiang, M. E. Minunni, A. P. F. Turner and M. Mascini, *Biosens. Bioelectron.*, 2005, **20**, 2310–2313.

7 S.-i. Nakano, T. Kanzaki, M. Nakano, D. Miyoshi and N. Sugimoto, *Anal. Chem.*, 2011, **83**, 6368–6372.

8 L. G. Carrascosa, A. Calle and L. M. Lechuga, *Anal. Bioanal. Chem.*, 2009, **393**, 1173–1182.

9 S. S. Aćimović, M. A. Ortega, V. Sanz, J. Berthelot, J. L. Garcia-Cordero, J. Renger, S. J. Maerkl, M. P. Kreuzer and R. Quidant, *Nano Lett.*, 2014, **14**, 2636–2641.

10 M. Poksinski and H. Arwin, *Thin Solid Films*, 2004, **455–456**, 716–721.

11 A. V. Nabok, A. Tsargorodskaya, A. K. Hassan and N. F. Starodub, *Appl. Surf. Sci.*, 2005, **246**, 381–386.

12 H. Arwin, M. Poksinski and K. Johansen, *Appl. Opt.*, 2004, 3028–3036.

13 R. S. Moirangthem, Y.-C. Chang, S.-H. Hsu and P.-K. Wei, *Biosens. Bioelectron.*, 2010, **25**, 2633–2638.

14 Z. Üstündağ, M. O. Cağlayan, R. Güzel, E. Pişkin and A. O. Solak, *Analyst*, 2011, **136**, 1464–1471.

15 P. K. Jain, X. Huang, I. H. El-Sayed and M. A. El-Sayed, *Plasmonics*, 2007, **2**, 107–118.

16 K. A. Willets and R. P. V. Duyne, *Annu. Rev. Phys. Chem.*, 2007, **58**, 267–297.

17 X. Lan, Z. Chen, B.-J. Liu, B. Ren, J. Henzie and Q. Wang, *Small*, 2013, **9**, 2308–2315.

18 H. M. Chen, C. K. Chen, M. L. Tseng, P. C. Wu, C. M. Chang, L.-C. Cheng, H. W. Huang, T. S. Chan, D.-W. Huang, R.-S. Liu and D. P. Tsai, *Small*, 2013, **9**, 2926–2936.

19 E. Hutter and J. H. Fendler, *Adv. Mater.*, 2004, **16**, 1685–1706.

20 P. C. Wu, T.-H. Kim, A. S. Brown, M. Losurdo, G. Bruno and H. O. Everitt, *Appl. Phys. Lett.*, 2007, **90**, 103119.

21 P. Albella, B. Garcia-Cueto, F. González, F. Moreno, P. C. Wu, T.-H. Kim, A. Brown, Y. Yang, H. O. Everitt and G. Videen, *Nano Lett.*, 2011, **11**, 3531–3537.

22 Y. Yang, J. M. Callahan, T.-H. Kim, A. S. Brown and H. O. Everitt, *Nano Lett.*, 2013, **13**, 2837–2841.

23 M. Yarema, M. Wörle, M. D. Rossell, R. Erni, R. Caputo, L. Protesescu, K. V. Kravchyk, D. N. Dirin, K. Lienau, F. von Rohr, A. Schilling, M. Nachtegaal and M. V. Kovalenko, *J. Am. Chem. Soc.*, 2014, **136**, 12422–12430.

24 M. W. Knight, T. Coenen, Y. Yang, B. J. M. Brenny, M. Losurdo, A. S. Brown, H. O. Everitt and A. Polman, *ACS Nano*, 2015, **9**, 2049–2060.

25 R. Verre, M. Modreanu, O. Ualibek, D. Fox, K. Fleischer, C. Smith, H. Zhang, M. Pemble, J. F. McGilp and I. V. Shvets, *Phys. Rev. B: Condens. Matter*, 2013, **87**, 235428.

26 A. García Marín, M. J. Hernández, E. Ruiz, J. M. Abad, E. Lorenzo, J. Piqueras and J. L. Pau, *Biosens. Bioelectron.*, 2015, **74**, 1069–1075.

27 B. Kerem, J. M. Rommens, J. A. Buchanan, D. Markiewicz, T. K. Cox, A. Chakravarti, M. Buchwald and L. C. Tsui, *Science*, 1989, **245**, 1073–1080.

28 A. Di Cicco, *Phys. Rev. Lett.*, 1998, **81**, 2942–2945.

29 H. G. Tompkins, *A User's Guide to Ellipsometry*, Academic Press, 1993.

30 P. C. Wu, M. Losurdo, T.-H. Kim, M. Giangregorio, G. Bruno, H. O. Everitt and A. S. Brown, *Langmuir*, 2009, **25**, 924–930.

31 D. Tonova, M. Patrini, P. Tognini, A. Stella, P. Cheyssac and R. Kofman, *J. Phys.: Condens. Matter*, 1999, **11**, 2211–2222.

32 M. J. Hernández, M. Cervera, E. Ruiz, J. L. Pau, J. Piqueras, M. Avella and J. Jiménez, *Nanotechnology*, 2010, **21**, 455602.

33 P. C. Wu, T.-H. Kim, A. Suvorova, M. Giangregorio, M. Saunders, G. Bruno, A. S. Brown and M. Losurdo, *Small*, 2011, **7**, 751–756.

34 T. M. Herne and M. J. Tarlov, *J. Am. Chem. Soc.*, 1997, **119**, 8916–8920.

35 T. García-Mendiola, T. Barreiro Martínez, F. Pariente, J. Molano and E. Lorenzo, *Electroanalysis*, 2014, **26**, 1362–1372.

36 D.-W. Pang, Y.-P. Qi, Z.-L. Wang, J.-K. Cheng and J.-W. Wang, *Electroanalysis*, 1995, **7**, 774–777.